

Object Pose Distribution Estimation for Determining Revolution and Reflection Uncertainty in Point Clouds

1st Frederik Hagelskjær*

*SDU Robotics
The Mærsk Mc-Kinney
Møller Institute*

*University of Southern Denmark
Odense, Denmark
frhag@mmmi.sdu.dk*

*Corresponding author

2nd Dimitrios Arapis

*Finished Product
Manufacturing
Science & Technology*

*Novo Nordisk A/S
Hillerød, Denmark
dtai@novonordisk.com*

3rd Steffen Madsen

*Finished Product
Manufacturing
Science & Technology*

*Novo Nordisk A/S
Hillerød, Denmark
bfma@novonordisk.com*

4th Thorbjørn Mosekjær Iversen

*SDU Robotics
The Mærsk Mc-Kinney
Møller Institute*

*University of Southern Denmark
Odense, Denmark
thmi@mmmi.sdu.dk*

Abstract—Object pose estimation is crucial to robotic perception and typically provides a single-pose estimate. However, a single estimate cannot capture pose uncertainty deriving from visual ambiguity, which can lead to unreliable behavior. Existing pose distribution methods rely heavily on color information, often unavailable in industrial settings.

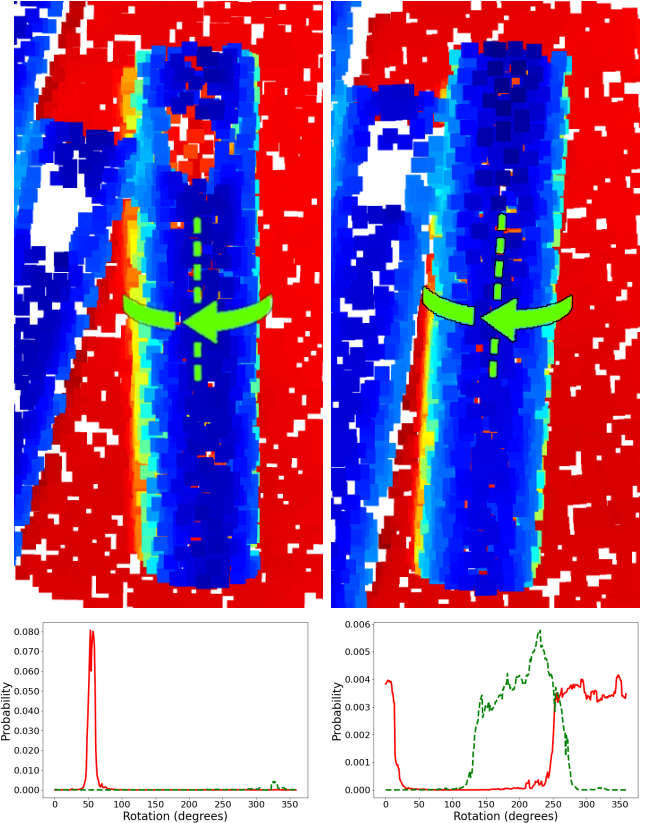
We propose a novel neural network-based method for estimating object pose uncertainty using only 3D colorless data. To the best of our knowledge, this is the first approach that leverages deep learning for pose distribution estimation without relying on RGB input. We validate our method in a real-world bin picking scenario with objects of varying geometric ambiguity. Our current implementation focuses on symmetries in reflection and revolution, but the framework is extendable to full $SE(3)$ pose distribution estimation. Source code available at [opde3d.github.io](https://github.com/opde3d)

Index Terms—pose uncertainty, pose estimation, point cloud

I. INTRODUCTION

Recent advances in manufacturing technology have introduced a shift from traditional mass production toward small-batch and one-of-a-kind manufacturing. Additive manufacturing and autonomous robotic assembly are key drivers in this transformation [1], [2]. Flexible fabrication solutions allow for customization, rapid prototyping, and decentralized production. Object pose estimation (OPE) plays an important role in flexible robotic assembly, as it enables systems to adapt to novel objects without requiring physical redesign [3]. The general approach in OPE is a single-pose estimate [4]–[7]. Single-pose estimates align well with many robotic systems, as they enable direct transformation chaining, where components such as camera extrinsics, object poses, and robot TCPs can be linked in a kinematic chain. This enables straightforward computation of grasp poses or end-effector targets using simple matrix multiplications. However, single-pose estimates are not able to model the aleatoric uncertainty that occurs when visual ambiguity is present. One example of visual ambiguity is seen in many industrial objects, such as idlers, bearings, and screws, which exhibit cylindrical symmetry [3], [8]. Here, the cylindrical shape results in an ambiguity about

This project was funded in part by Innovation Fund Denmark through the projects MADE ReAct and FERA, and in part by the SDU I4.0-Lab.



(c) View where the square recess is distinguishable. The pose distribution is a single peak with low uncertainty in prediction. (d) Rotated view without any distinguishing features. The pose distribution is larger with uncertainty in both revolution and reflection.

Fig. 1. The pose distribution estimate of our method is shown for both unambiguous and ambiguous views. The top images display the test object in two different poses. Below, the distribution estimates are visualized. The red line indicates the probability of each revolution. The dotted green line shows the same revolution probability for the reflected pose. In the left image, the object's indent is visible, allowing for a single object pose to be identified. In the right image, the indent is not visible, resulting in a much larger pose distribution in both revolution and reflection.

the correct reflection and revolution of the object. For some tasks, pose ambiguity is not relevant to the task's success; however, ignoring pose ambiguity can often lead to failures, potentially damaging the object, equipment, or the robot. To

avoid this, extensive checks with additional hardware can be made [9]. But detecting such ambiguities and correcting them is an expensive engineering task that does not align well with flexible systems handling new assemblies with novel objects.

This limitation of single-pose estimates has led to work on estimating object pose distributions [10]–[12]. In these works, the method estimates a probability distribution over poses, formalized as a histogram. This histogram can then be used to determine the certainty of a given pose. However, all of these methods focus on RGB images for input. But, in many industrial scenarios, 3D sensors are used because color information is either unavailable or unreliable. Additionally, by only relying on 3D data the method becomes independent of lighting conditions. To address this gap, we introduce an object pose distribution estimator that operates solely on 3D data.

The method is an adaptation of the RGB-based SpyroPose [11] sampling to 3D point clouds. This is achieved by a introducing a feature aggregator that combines spatial and embedding information. To the best of our knowledge, this is the first work to estimate object pose distribution histograms in point clouds using neural networks.

In this paper, we restrict the search space to reflection and revolution. This restriction enables us to generate a complete histogram of rotational uncertainty using our network. Using this, we can define clear rules for interpreting the uncertainty. For example, we may require a single normally distributed estimate, disallow reflection when not physically plausible, or allow revolution symmetry only at specified angular intervals. This restriction is possible because we rely on 3D data and focus on cylindrical objects. For such objects, most uncertainty can be removed using verification by depth projection [9], [13]. However, because of inherent symmetry, depth verification cannot resolve ambiguities in rotation around or reflection across the symmetry axis. As a result, revolution and reflection remain the primary sources of pose uncertainty, and the focus of the uncertainty estimate in this paper. We demonstrate the effectiveness of this approach in a bin picking scenario. An existing point estimator provides an initial pose, and our method estimates the pose distribution. This enables us to correctly identify ambiguous poses and avoid incorrect grasps, improving reliability and robustness.

The main contributions presented in this paper are:

- A method for determining revolution and reflection uncertainty in point clouds
- A feature aggregator for computing pose likelihoods in point clouds
- Verification in a real bin picking scenario

We believe this paper will inspire further work in object pose distribution estimation in point clouds.

II. RELATED WORKS

Visual ambiguities and aleatoric uncertainty are challenging aspects in object pose estimation (OPE). Benchmark datasets typically address this by manually annotating symmetries,

thereby requiring only a single-pose estimate for evaluating pose correctness [8], [14]–[16].

To mitigate ambiguity in practice, a common strategy in OPE is to generate per-pixel histograms of object correspondences. These 2D–3D correspondences are then processed using PnP-RANSAC [17] to compute a final pose. This approach has significantly improved robustness [18], [19], and is currently employed by leading methods in the BOP benchmark [14], [20]. However, despite its effectiveness, it remains unclear how to translate per-point distributions into a coherent pose distribution.

A. Distributions in RGB data

Methods for estimating pose distributions have been actively explored in recent years. For example, [21] presents an approach where synthetic images are used to estimate the uncertainty of pose estimates. This uncertainty is modeled using a Gaussian distribution and integrated with a simulation of grasping success under pose errors. The resulting framework enables the design of grippers that are robust to OPE uncertainty.

Orientation uncertainty has also been modeled using Bingham and von-Mises distributions [22], [23]. These parametric models are effective for representing unimodal distributions and have been widely adopted in robotics and computer vision. However, their ability to capture complex uncertainty is limited. Specifically, they cannot represent multimodal uncertainties, such as multiple plausible orientations in visually ambiguous scenes, e.g., when objects exhibit symmetry or are partially occluded.

To address these limitations un-parametric, implicit models have been developed. Using an image crop of the object Ki-Pode [24], computes heatmaps representing the confidence of each objects keypoint’s position. By projecting the object onto these heatmaps an un-normalized likelihood of a given pose can be approximated. Another approach is shown in ImplicitPDF [10] where an image embedding is combined with a rotation, and then fed to a network which provides an un-normalized likelihood of the rotation. In both cases normalized using equivolumetric sampling of $SO(3)$ is used to provide a normalized likelihood.

SpyroPose [11] computes image embeddings which are then extracted using projected keypoints and processed by a Multi Layer Perceptron (MLP). As the keypoints are transformed using a pose this allow for pose distribution in 6 Degrees of Freedom (DoF). However, introducing 6 DoF creates a very large search space. To avoid exhaustive computation, a pyramid approach is used. Starting at an equivolumetric grid at the lowest resolution, followed by importance sampling, this enables SpyroPose to provide pose distributions in $SE(3)$. Similarly to SpyroPose our method extracts embedding in the scene using keypoints. But, as our data is a 3D point cloud nearest neighbor is used instead of the camera projection. In this paper, we do not estimate distributions in $SE(3)$, but only compute uncertainty in revolution and reflection.

A different method for estimating the uncertainty in $SE(3)$ is presented in Lie [25]. Here a diffusion model is used to represent uncertainty. By using a sampling based strategy the set of poses is recovered.

B. Distributions in 3D data

Similar to RGB-based approaches, point cloud methods have employed per-point histograms of object correspondences to enhance OPE. A common technique for computing the pose is Kabsch-RANSAC [17], [29], which robustly estimates transformations but does not yield pose distributions.

To refine the pose, the standard method is Iterative Closest Point (ICP) [30]. ICP iteratively minimizes the distance between object and scene point clouds to improve alignment. While ICP itself does not provide uncertainty estimates. Due to its widespread use, several extensions have been proposed to incorporate uncertainty into ICP-based pose estimation [31]–[35]. However, ICP has inherent limitations. As it relies solely on geometric matching it does not leverage learned features or contextual knowledge. As a result, it is sensitive to noise and missing data, especially in cases where semantic cues could aid matching. This lack of learned parameters restricts its robustness in complex or ambiguous scenes. This is the same limitation observed with the depth check employed in the initial pose estimation [9], [36].

III. METHOD

The proposed method comprises three core components: a feature encoder, a keypoint feature extractor, and an MLP for scoring. While the overall architecture is inspired by SpyroPose [11], several modifications have been introduced to accommodate 3D data.

A. Problem Definition

Given a set of sample transforms, T_{sample} , and a point cloud, compute the likelihood of each sample transform being the correct pose. The set of sample transforms is obtained by combining an initial pose estimate, T_{init} , with a set of sample rotations. The sample rotations are used to test for full axial symmetry and reflection. The computation of the sample transforms is shown in Eq. (1). Where θ_{ref} is either zero or 180° and θ_{revo} goes from zero to 359° .

$$T_{sample} = R_y(\theta_{ref})R_z(\theta_{revo})T_{init} \quad (1)$$

For each transform, an un-normalized likelihood is computed, and by normalizing across all rotations, the probability of each transform is determined.

B. Object Keypoints

Before the network is trained, keypoints are sampled from the CAD model. The keypoints are found similarly to SpyroPose, by using farthest point sampling on the CAD model. In our experiments, we use 32 keypoints, which are sampled only once and remain consistent throughout both the training and test phases.

C. Feature Encoding

Firstly, the scene is encoded using a neural network. We employ a PointNet-like structure, as they have shown very good performance in encoding point cloud data [26]–[28]. In this paper, we use DGCNN [27] pre-trained from KeyMatchNet [37], but it could be exchanged with any PointNet-like network [26]–[28], [38], [39].

The input to the network is a colorless point cloud with six dimensions, consisting of position and normal vectors. The point cloud has a size of 4096. Before processing the point cloud, it is normalized by centering around the object center and scaled by the object radius. For DGCNN, the number of neighbors is set to twenty.

D. Keypoint Nearest Neighbor Sampling

From the encoded point cloud, the feature points are then sampled by finding the nearest points to the keypoint set. The keypoint set is computed by transforming the keypoints by the sample transforms, T_{sample} . Thus, nearest neighbors are found for all the object poses in the sample transform set. The nearest neighbor is computed using the Euclidean distance between the transformed keypoints and the scene point cloud.

The feature encoding for the nearest point is then used as the feature embedding of the keypoint, f_j . As point cloud data also includes spatial information, we incorporate this data as well. Thus, for each keypoint, the spatial difference between the keypoint, x_i , and the nearest neighbor, x_j , is computed. The embedding and spatial difference are then supplied to the Keypoint Feature Aggregator.

E. Keypoint Feature Aggregator

The keypoint feature aggregator ensures that the spatial information, $x_i - x_j$, is encoded together with the feature encoding, f_j . This is achieved by processing both features through an MLP, which results in two 64-dimensional feature vectors, h_x and h_f , respectively. These feature vectors are then concatenated and processed by an MLP, \hat{h} , returning a size 64 feature vector. The feature computation is shown in Eq. (2).

$$\hat{h}(h_x(x_i - x_j) \oplus h_f(f_j)) \quad (2)$$

Finally, all keypoint features are concatenated into a single feature vector. This vector is then processed by a three-layer MLP with 256 hidden neurons.

F. Training

The network is trained using ADAM optimizer [40] with a learning rate of 10^{-4} . The network is trained using the InfoNCE loss [41] for 4,000 epochs, with 1,000 batches per epoch and a batch size of one. For the three-layer MLP, dropout and point-dropout are both applied. The dropout rate is set to 10%.

During training, we utilize data augmentation to enhance generalization. We impose a 1 mm normally distributed error on the object translation, and for the two non-revolutionary axes, a 3-degree variance. On the revolutionary axis, we

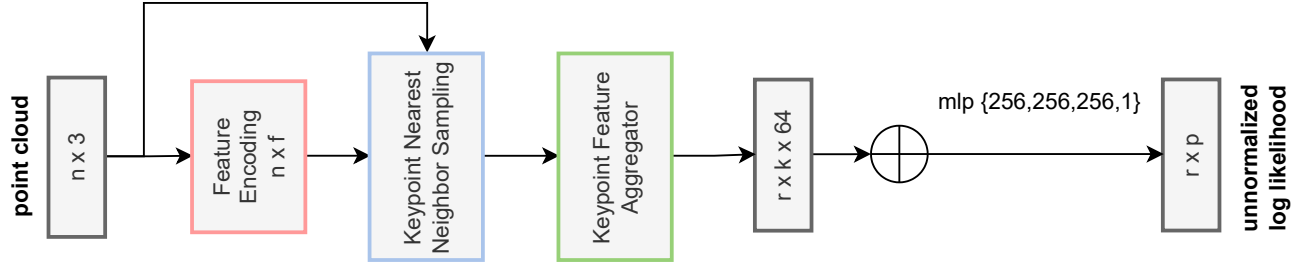


Fig. 2. The structure of the developed network. "Feature Encoding" is performed using a PointNet [26] structure (e.g. DGCNN [27], PointNet++ [28]). "n" is the size of the input point cloud, "f" is the size of the feature vector from the "Feature Encoding", "r" is the number of sample rotations, and "k" is the number of keypoints.

use a variance of 0.5 degrees. The depth data is augmented according to the strategy in [42].

G. Inference

When running the method for inference, the initial pose estimate T_{init} must be provided from an external method. Using the pose estimate, the point cloud is then cropped and normalized. The point cloud and initial pose estimate are then fed to the method, which returns the un-normalized log likelihood of all sample rotations. Finally, a softmax is applied to obtain the pose distribution.

H. Applying the Pose Distribution

The computed pose distribution is represented as a histogram, indicating the probability that each sampled rotation corresponds to the correct pose. To apply this in practice, it is necessary to define a strategy that determines what level or type of uncertainty is acceptable for a given task.

One straightforward strategy is to require that the pose distribution fit within a single pose. For certain tasks, this constraint is critical to maintaining reliable system performance. For other tasks, the requirement is the absence of uncertainty in reflection, which aligns well with many screw-like objects [3]. Alternatively, another approach is to accept symmetric rotations, as seen in gears and nuts [16]. Depending on the task, these symmetric rotations may be acceptable with or without uncertainty in reflection. In our experiments, we evaluate both strategies: enforcing a single-pose estimate and ensuring the absence of reflection. In contrast to the above, a different approach involves determining acceptable uncertainty through simulation [21], [43]. Task execution can be simulated using various grasp poses, allowing the error rate to be integrated with the pose distribution. This provides a probabilistic estimate of task failure given a specific pose distribution.

Handling pose distributions with excessive uncertainty is another important consideration. For some tasks, objects outside the defined threshold can be skipped. For other tasks, a strategy must be specified, such as obtaining new views, reorienting the object, or using physical manipulation to gather new data [9], [43].

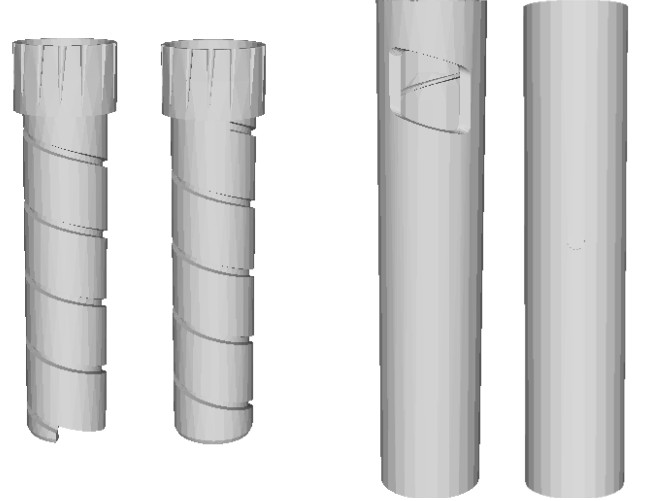


Fig. 3. Front and back views of the two objects from our experiments. For Object 1 (left) the correct revolution can only be precisely determined from the indent at the bottom, but the reflection can easily be seen from the screw-head. However, for Object 2 (right) both reflection and revolution can only be determined from the square recess. Thus in case of self occlusion the correct reflection is ambiguous.

IV. EXPERIMENTS

To evaluate the effectiveness of our method, we conduct experiments with two different objects, using both synthetic and real test data. Finally, we implement the method on the real setup and test the grasping performance.

All experiments were performed on a PC environment (Intel Ultra 7 155H CPU and NVIDIA RTX 1000 Ada Generation Laptop GPU). Depth augmentation were performed using OpenCV [44], point clouds were processed using Open3D [45] and networks were implemented using PyTorch [46].

A. Objects

The objects are components of a Novo Nordisk injection device and part of an assembly process, as described in [9], [36]. Both are shown in Fig. 3. Successful insertion requires knowledge of the correct orientation. For Object 1, only the correct reflection is required, while Object 2 also necessitates precise rotational alignment. Object 2 is particularly challeng-



Fig. 4. Synthetic image of Object 2.

TABLE I
RESULTS FOR PREDICTION OF REFLECTION AND POSE FOR THE
SYNTHETIC TEST DATA.

Object	Instances	Task	Coverage (%)	Precision (%)
1	2140	Reflection	98.8	100
		Pose	45.7	100
2	1743	Reflection	58.9	100
		Pose	32.7	100

ing, as self-occlusion of the square recess can prevent accurate pose estimation.

B. Synthetic Data

For experiments with synthetic data, the depth data is generated using BlenderProc [47]. We create 2,000 scenes, of which 100 are retained for testing. Similar to [48], we require that the object have at least 50% visibility, as objects with less visibility generally do not result in stable grasps. This results in 40,459 and 31,622 training instances for objects 1 and 2, respectively, with 2140 and 1743 test instances. An example of the synthetic data is shown in Fig. 4.

We test for the ability to correctly classify reflection and the full pose with revolution. The cut-off for accepting a prediction is 99% confidence inside the prediction. For reflection, this is set to the full rotation, and for the full pose, we accept a 15° range.

The results of the experiments are shown in Tab. I. From the results, it is seen that our method is able to avoid making predictions in ambiguous scenes and obtain a precision of 100%. For the two objects, the coverage, however, is quite different. The reflection is found for almost all cases for Object 1, whereas it is only predicted in 58.9% of cases for Object 2. This is a result of self-occlusion, which means that even with perfect data, the correct orientation is often ambiguous.

C. Bin Picking Data

In the existing set-up pose estimates were obtained using KeyMatchNet [37], and incorrect poses were filtered out using a depth check with a threshold of 2.5, mm. An example of the bins is shown in Fig. 5. However, in cases of visual ambiguity, single-pose estimates do not convey the pose uncertainty. To



Fig. 5. Example of Object 2 in the bins.

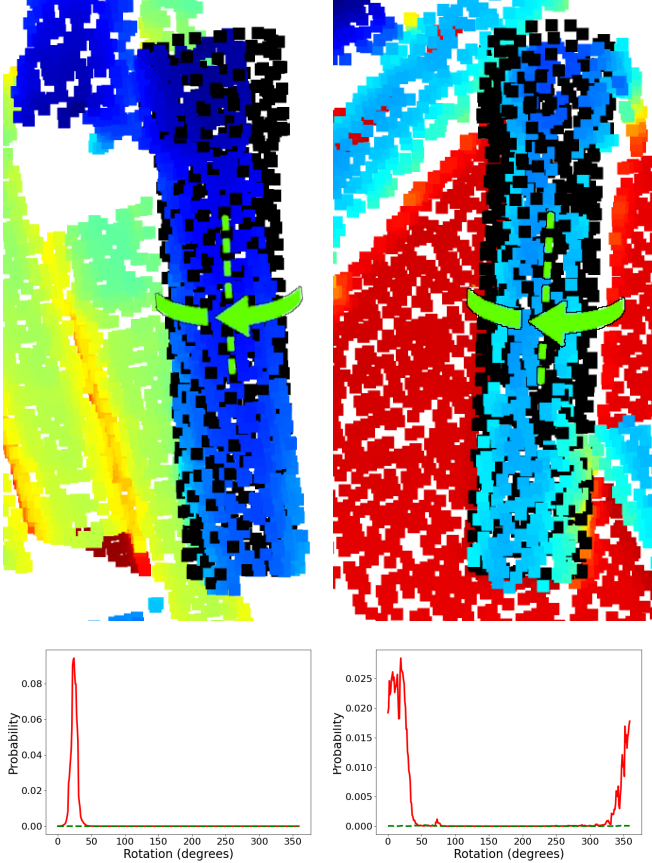
ensure accurate pose estimation, the system performs an in-hand pose check. This procedure is time-consuming, and for Object 2, it still results in ambiguous reflection estimation. Consequently, an additional fixture check was implemented [36]. The pose estimation from the system resulted in incorrect reflection estimates of 86.4% and 53.8% for Object 1 and Object 2, respectively.

We test our method using the real data collected from the set-up [9]. The training data is the same synthetic data from the previous section. The result of our method on the real data is presented in Table II. For all objects in the test set, the precision is 100%. However, task coverage varies significantly. For Object 1, reflection prediction coverage is 87%, which is substantially higher than the 4.5% coverage for full pose prediction. This discrepancy likely stems from noise in the real data. As the grooves on the object are not visible, only the bottom indent can be used to determine revolution. Due to noise interference, only a few samples achieve sufficient confidence. Real test data for Object 1 is shown in Fig. 6. For Object 2, the coverage of both tasks is more balanced, as the square recess must be visible to determine either. Although the coverage is lower, it remains within a usable range.

With 100% precision across all tasks and objects, the system can operate autonomously without requiring additional engineering solutions such as a second camera or mechanical verification. This enables flexible production setups where new objects, such as those from additive manufacturing, can be integrated remotely. The overall recall for correct reflection estimation, disregarding distribution requirements, is 98% for Object 1 and 80% for Object 2. These results significantly outperform current systems, suggesting that our approach could enhance existing setups with engineered checks.

TABLE II
RESULTS FOR PREDICTION OF REFLECTION AND POSE FOR THE REAL TEST DATA.

Object	Instances	Task	Coverage (%)	Precision (%)
1	200	Reflection	87	100
		Pose	4.5	100
2	200	Reflection	43	100
		Pose	31	100



(c) View where the tack at the bottom is visible. Resulting in a single peak prediction. (d) View without the tack at the bottom visible. Resulting in a larger uncertainty in pose.

Fig. 6. The pose distribution estimate of our method visualized, for two instances of Object 1. When the tack at the bottom is not visible, the pose distribution becomes larger.

D. Bin Picking Test

To test the effectiveness of the developed method in a bin picking scenario, we implemented the algorithm on a real setup. We compare our method with the existing system, which relies on a second camera for in-hand pose estimation and a fixture for verification. As our method returns the complete pose distribution, we do not rely on either of these additional steps. However, if all object poses are uncertain, the system cannot perform any grasps. To ensure that all objects can be grasped and inserted, we develop a re-orientation strategy. First, all object poses are found, and if none of the poses are certain, an object is grasped and flipped into a random

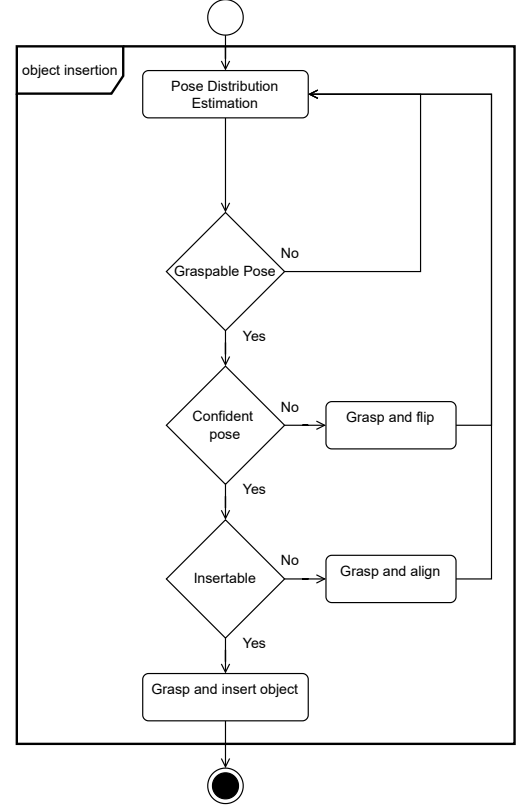


Fig. 7. Activity diagram of the bin picking process using confidence intervals. If no object poses with high confidence are available the robot grasps an object and reorients it.

TABLE III
RESULTS FOR BIN PICKING OF 10 OBJECTS. COMPARISON WITH THE ORIGINAL SETUP.

Method	Grasps	Incorrect Insertions	Failures
Previous	18	8	0
Ours	20	0	0

position. If a pose is certain, but the resulting grasp is not usable for insertion, the object is aligned so that it can be inserted in the next grasp. Finally, if the pose is confident and the object can be inserted, this is simply performed. This bin picking strategy is shown in Fig. 7.

For both methods, we operated the system until 10 successful insertions were completed. The results appear in Tab. III. From these results, several key observations emerge. First, both methods achieved insertions without critical failures. Our method required 20 grasps to accomplish 10 insertions, resulting from five rotation adjustments and five object flips. This slightly exceeds the 18 grasps required by the original setup. Crucially, our system did not produce any incorrect insertions, indicating that supplemental hardware and software components are unnecessary. In two alignments, the resulting pose was not suitable for insertion. System performance could be enhanced by adopting improved alignment strategies.

E. Additive Manufacturing

To assess the algorithm's effectiveness in an additive manufacturing context, we used a 3D-printed version of the object



Fig. 8. Example of the 3D printed test object.

TABLE IV
ABLATION STUDY RESULTS FOR PREDICTION OF REFLECTION AND POSE FOR OBJECT 2 ON THE SYNTHETIC TEST DATA.

Omitted	Instances	Task	Coverage (%)	Precision (%)
None	1743	Reflection	58.9	100
		Pose	32.7	100
Spat.	1743	Reflection	56.0	100
		Pose	29.9	99.8
Feat.	1743	Reflection	0	N/A
		Pose	0	N/A

made from a semi-transparent material. An example of the printed test object is shown in Fig. 8. The test was performed using the grasping strategy introduced above. The system executed ten successful insertions without any errors. All ambiguous poses were consistently reoriented until insertions could be performed.

F. Ablation Study

To test the contribution of the different parts of the feature aggregator, an ablation study is performed. We train a version of the model excluding either the spatial information or the feature encoding. We test the network’s performance on the synthetic test data for object 2. The results are shown in Tab. IV. From the results, it is evident that combining the features yields better performance than using the feature encoding alone. It is also observed that, by using only spatial information, the network is unable to learn a representation of pose uncertainty.

G. Run-time

Another aspect of the algorithm’s usability is its run-time. The run-time of each part of the algorithm is shown in Tab. V. The cumulative run-time for a single object is 32.5 milliseconds. This would enable near real-time processing of objects during the robot’s operation.

An important factor for further development is the run-time for the pose sampling. If the method were extended to cover $SE(3)$, this part would increase, whereas the run-time for loading point clouds and feature encoding would remain static. The cumulative time for sampling the 720 poses is 2.1 milliseconds. This is a small part of the full run-time and would allow the algorithm to be used for estimating uncertainty in $SE(3)$.

V. CONCLUSION AND FUTURE WORK

In this paper, we present a method for estimating object pose distributions in 3D point clouds. Our method estimates uncertainty in revolution and reflection. Tests were conducted

TABLE V
THE RUN-TIME OF A SINGLE PASS OF THE ALGORITHM.

Task	Time [ms]	Cum. Time [ms]
Loading point cloud	25.5	25.5
Feature Encoding	4.9	30.4
Nearest Neighbor	0.2	30.6
Feature Aggregator	0.7	31.3
Model Head	1.3	32.5

on two objects from a bin picking scenario. The method was also implemented on a real system and used for grasping. Experiments demonstrate that the method can model the uncertainty arising from visual ambiguities. Thus, our method does not make any incorrect pose predictions and can be used reliably in uncertain environments. This will enable more robust and flexible robotic applications that can still operate correctly in the presence of visual ambiguity.

In further work, the method can be extended to $SE(3)$ distributions to cover full 6 DoF pose uncertainty estimation. This will require sampling and training similar to SpyroPose [11], but the network structure would not have to be changed. Additionally, the method could be tested on benchmark datasets and potentially compared with RGB-based methods. Another topic for future research is to evaluate the impact of different feature encoders. We have used the well-known DGCNN [27], but several others could be used. Color information could also be incorporated to test the effectiveness of a multi-modal encoder.

ACKNOWLEDGMENT

The authors gratefully acknowledge the helpful discussions and feedback provided by Rasmus Laurvig Haugaard.

REFERENCES

- [1] E. Dalpadulo, A. Petruccioli, F. Gherardini, and F. Leali, “A review of automotive spare-part reconstruction based on additive manufacturing,” *Journal of Manufacturing and Materials Processing*, vol. 6, no. 6, p. 133, 2022.
- [2] G. Prashar, H. Vasudev, and D. Bhuddhi, “Additive manufacturing: expanding 3d printing horizon in industry 4.0,” *International Journal on Interactive Design and Manufacturing (IJIDeM)*, vol. 17, no. 5, pp. 2221–2235, 2023.
- [3] Y. Yokokohji, Y. Kawai, M. Shibata, Y. Aiyama, S. Kotosaka, W. Uemura, A. Noda, H. Dobashi, T. Sakaguchi, and K. Yokoi, “Assembly challenge: a robot competition of the industrial robotics category, world robot summit—summary of the pre-competition in 2018,” *Advanced Robotics*, vol. 33, no. 17, pp. 876–899, 2019.
- [4] T. Hodan, F. Michel, E. Brachmann, W. Kehl, A. GlentBuch, D. Kraft, B. Drost, J. Vidal, S. Ihrke, X. Zabulis *et al.*, “Bop: Benchmark for 6d object pose estimation,” in *Proceedings of the European conference on computer vision (ECCV)*, 2018, pp. 19–34.
- [5] T. Hodan, M. Sundermeyer, B. Drost, Y. Labbé, E. Brachmann, F. Michel, C. Rother, and J. Matas, “Bop challenge 2020 on 6d object localization,” in *Computer Vision—ECCV 2020 Workshops: Glasgow, UK, August 23–28, 2020, Proceedings, Part II 16*. Springer, 2020, pp. 577–594.
- [6] M. Sundermeyer, T. Hodan, Y. Labbe, G. Wang, E. Brachmann, B. Drost, C. Rother, and J. Matas, “Bop challenge 2022 on detection, segmentation and pose estimation of specific rigid objects,” *arXiv preprint arXiv:2302.13075*, 2023.
- [7] T. Hodan, M. Sundermeyer, Y. Labbe, V. N. Nguyen, G. Wang, E. Brachmann, B. Drost, V. Lepetit, C. Rother, and J. Matas, “Bop challenge 2023 on detection segmentation and pose estimation of seen and unseen rigid objects,” in *Proceedings of the IEEE/CVF Conference on Computer Vision and Pattern Recognition*, 2024, pp. 5610–5619.

- [8] K. Kleeberger, C. Landgraf, and M. F. Huber, "Large-scale 6d object pose estimation dataset for industrial bin-picking. in 2019 IEEE," in *RSJ International Conference on Intelligent Robots and Systems (IROS)*, 2019, pp. 2573–2578.
- [9] F. Hagelskjær, "Good grasps only: A data engine for self-supervised fine-tuning of pose estimation using grasp poses for verification," in *2025 IEEE/SICE International Symposium on System Integration (SII)*. IEEE, 2025, pp. 957–964.
- [10] K. Murphy, C. Esteves, V. Jampani, S. Ramalingam, and A. Makadia, "Implicit-pdf: Non-parametric representation of probability distributions on the rotation manifold," *arXiv preprint arXiv:2106.05965*, 2021.
- [11] R. L. Haugaard, F. Hagelskjær, and T. M. Iversen, "Spyropose: Se (3) pyramids for object pose distribution estimation," in *Proceedings of the IEEE/CVF International Conference on Computer Vision*, 2023, pp. 2082–2091.
- [12] A. Brazi, B. Meden, F. M. de Chamisso, S. Bourgeois, and V. Lepetit, "Corr2distrib: Making ambiguous correspondences an ally to predict reliable 6d pose distributions," *IEEE Robotics and Automation Letters*, 2025.
- [13] F. Hagelskjær, D. Kraft *et al.*, "Off-the-shelf bin picking workcell with visual pose estimation: A case study on the world robot summit 2018 kitting task," in *2024 21st International Conference on Ubiquitous Robots (UR)*. IEEE, 2024, pp. 145–152.
- [14] V. N. Nguyen, S. Tyree, A. Guo, M. Fourmy, A. Gouda, T. Lee, S. Moon, H. Son, L. Ranfil, J. Tremblay *et al.*, "Bop challenge 2024 on model-based and model-free 6d object pose estimation," *arXiv preprint arXiv:2504.02812*, 2025.
- [15] A. Doumanoglou, R. Kouskouridas, S. Malassiotis, and T.-K. Kim, "Recovering 6d object pose and predicting next-best-view in the crowd," in *Proceedings of the IEEE conference on computer vision and pattern recognition*, 2016, pp. 3583–3592.
- [16] J. Yang, Y. Gao, D. Li, and S. L. Waslander, "Robi: A multi-view dataset for reflective objects in robotic bin-picking," in *2021 IEEE/RSJ International Conference on Intelligent Robots and Systems (IROS)*. IEEE, 2021, pp. 9788–9795.
- [17] M. A. Fischler and R. C. Bolles, "Random sample consensus: a paradigm for model fitting with applications to image analysis and automated cartography," *Communications of the ACM*, vol. 24, no. 6, pp. 381–395, 1981.
- [18] T. Hodan, D. Barath, and J. Matas, "Epos: Estimating 6d pose of objects with symmetries," in *Proceedings of the IEEE/CVF conference on computer vision and pattern recognition*, 2020, pp. 11 703–11 712.
- [19] R. L. Haugaard and A. G. Buch, "Surfemb: Dense and continuous correspondence distributions for object pose estimation with learnt surface embeddings," in *Proceedings of the IEEE/CVF Conference on Computer Vision and Pattern Recognition*, 2022, pp. 6749–6758.
- [20] A. Caraffa, D. Boscaini, A. Hamza, and F. Poiesi, "Freeze: Training-free zero-shot 6d pose estimation with geometric and vision foundation models," in *European Conference on Computer Vision*. Springer, 2024, pp. 414–431.
- [21] F. Hagelskjær, A. Kramberger, A. Wolniakowski, T. R. Savarimuthu, and N. Krüger, "Combined optimization of gripper finger design and pose estimation processes for advanced industrial assembly," in *2019 IEEE/RSJ International Conference on Intelligent Robots and Systems (IROS)*. IEEE, 2019, pp. 2022–2029.
- [22] V. Peretroukhin, M. Giamou, D. M. Rosen, W. N. Greene, N. Roy, and J. Kelly, "A smooth representation of belief over so (3) for deep rotation learning with uncertainty," *arXiv preprint arXiv:2006.01031*, 2020.
- [23] S. Prokudin, P. Gehler, and S. Nowozin, "Deep directional statistics: Pose estimation with uncertainty quantification," in *Proceedings of the European conference on computer vision (ECCV)*, 2018, pp. 534–551.
- [24] T. M. Iversen, R. L. Haugaard, and A. G. Buch, "Ki-pode: Keypoint-based implicit pose distribution estimation of rigid objects," *arXiv preprint arXiv:2209.09659*, 2022.
- [25] T.-C. Hsiao, H.-W. Chen, H.-K. Yang, and C.-Y. Lee, "Confronting ambiguity in 6d object pose estimation via score-based diffusion on se (3)," in *Proceedings of the IEEE/CVF Conference on Computer Vision and Pattern Recognition*, 2024, pp. 352–362.
- [26] C. R. Qi, H. Su, K. Mo, and L. J. Guibas, "Pointnet: Deep learning on point sets for 3d classification and segmentation," in *Proceedings of the IEEE conference on computer vision and pattern recognition*, 2017, pp. 652–660.
- [27] Y. Wang, Y. Sun, Z. Liu, S. E. Sarma, M. M. Bronstein, and J. M. Solomon, "Dynamic graph cnn for learning on point clouds," *ACM Transactions on Graphics*, 2019.
- [28] C. R. Qi, L. Yi, H. Su, and L. J. Guibas, "Pointnet++: Deep hierarchical feature learning on point sets in a metric space," *Advances in neural information processing systems*, vol. 30, 2017.
- [29] W. Kabsch, "A solution for the best rotation to relate two sets of vectors," *Acta Crystallographica Section A: Crystal Physics, Diffraction, Theoretical and General Crystallography*, vol. 32, no. 5, pp. 922–923, 1976.
- [30] K. S. Arun, T. S. Huang, and S. D. Blostein, "Least-squares fitting of two 3-d point sets," *IEEE Transactions on Pattern Analysis and Machine Intelligence*, vol. PAMI-9, no. 5, pp. 698–700, 1987.
- [31] A. Censi, "An accurate closed-form estimate of icp's covariance," in *Proceedings 2007 IEEE international conference on robotics and automation*. IEEE, 2007, pp. 3167–3172.
- [32] T. M. Iversen, A. G. Buch, and D. Kraft, "Prediction of icp pose uncertainties using monte carlo simulation with synthetic depth images," in *2017 IEEE/RSJ International Conference on Intelligent Robots and Systems*. IEEE, 2017, pp. 4640–4647.
- [33] M. Brossard, S. Bonnabel, and A. Barrau, "A new approach to 3d icp covariance estimation," *IEEE Robotics and Automation Letters*, vol. 5, no. 2, pp. 744–751, 2020.
- [34] F. A. Maken, F. Ramos, and L. Ott, "Estimating motion uncertainty with bayesian icp," in *2020 IEEE International Conference on Robotics and Automation (ICRA)*. IEEE, 2020, pp. 8602–8608.
- [35] —, "Stein icp for uncertainty estimation in point cloud matching," *IEEE robotics and automation letters*, vol. 7, no. 2, pp. 1063–1070, 2021.
- [36] Z. Duan, F. Hagelskjær, A. Kramberger, J. Heredia, , and N. Krüger, "Towards high precision: An adaptive self-supervised learning framework for force-based verification," 2025. [Online]. Available: <https://arxiv.org/abs/2508.02153>
- [37] F. Hagelskjær and R. L. Haugaard, "Keymatchnet: Zero-shot pose estimation in 3d point clouds by generalized keypoint matching," in *2024 IEEE 20th International Conference on Automation Science and Engineering (CASE)*. IEEE, 2024, pp. 870–877.
- [38] H. Thomas, C. R. Qi, J.-E. Deschaud, B. Marcotegui, F. Goulette, and L. J. Guibas, "Kpconv: Flexible and deformable convolution for point clouds," in *Proceedings of the IEEE/CVF international conference on computer vision*, 2019, pp. 6411–6420.
- [39] H. Zhao, L. Jiang, J. Jia, P. H. Torr, and V. Koltun, "Point transformer," in *Proceedings of the IEEE/CVF international conference on computer vision*, 2021, pp. 16 259–16 268.
- [40] D. P. Kingma and J. Ba, "Adam: A method for stochastic optimization," *arXiv preprint arXiv:1412.6980*, 2014.
- [41] A. v. d. Oord, Y. Li, and O. Vinyals, "Representation learning with contrastive predictive coding," *arXiv preprint arXiv:1807.03748*, 2018.
- [42] F. Hagelskjær, "Arrowpose: Segmentation, detection, and 5 dof pose estimation network for colorless point clouds," *arXiv preprint arXiv:2506.08699*, 2025.
- [43] L. Naik, T. M. Iversen, A. Kramberger, and N. Krüger, "Robotic task success evaluation under multi-modal non-parametric object pose uncertainty," *Industrial Robot: the international journal of robotics research and application*, 2025.
- [44] G. Bradski, "The OpenCV Library," *Dr. Dobb's Journal of Software Tools*, 2000.
- [45] Q.-Y. Zhou, J. Park, and V. Koltun, "Open3D: A modern library for 3D data processing," *arXiv:1801.09847*, 2018.
- [46] A. Paszke, S. Gross, F. Massa, A. Lerer, J. Bradbury, G. Chanan, T. Killeen, Z. Lin, N. Gimelshein, L. Antiga, A. Desmaison, A. Kopf, E. Yang, Z. DeVito, M. Raison, A. Tejani, S. Chilamkurthy, B. Steiner, L. Fang, J. Bai, and S. Chintala, "PyTorch: An Imperative Style, High-Performance Deep Learning Library," in *Advances in Neural Information Processing Systems 32*, H. Wallach, H. Larochelle, A. Beygelzimer, F. d'Alché Buc, E. Fox, and R. Garnett, Eds. Curran Associates, Inc., 2019, pp. 8024–8035.
- [47] M. Denninger, M. Sundermeyer, D. Winkelbauer, Y. Zidan, D. Olefir, M. Elbadrawy, A. Lodhi, and H. Katam, "Blenderproc," *arXiv preprint arXiv:1911.01911*, 2019.
- [48] R. Brégier, F. Devernay, L. Leyrit, and J. L. Crowley, "Symmetry aware evaluation of 3d object detection and pose estimation in scenes of many parts in bulk," in *Proceedings of the IEEE International Conference on Computer Vision Workshops*, 2017, pp. 2209–2218.